Self-organized spatially separated silver 3D dendrites as efficient plasmonic nanostructures for Surface-enhanced Raman spectroscopy applications

Dzmitry V Yakimchuk[1], Egor Yu Kaniukov[2,3], Sergey Lepeshov[4], Victoria D Bundyukova[1], Sergey E Demyanov[1], Grigory M Arzumanyan[5,6], Nelya V Doroshkevich[6], Kahramon Z Mamatkulov[6], Arne Bochmann[7], Martin Presselt[8], Ondrej Stranik[8], Soslan A Khubezhov[9], Alex Krasnok[4,10], Andrea Alù[10,11,12], and Vladimir A Sivakov[8]

[1] Cryogenic Research Division, Scientific-Practical Materials Research Centre, NAS of Belarus, Minsk 220072, Belarus

[2] Institute of Chemistry of New Materials of National Academy of Sciences of Belarus, 36 St. Francyska Skaryny 220141 Minsk, Belarus

[3] Department of Electronics Materials Technology, National University of Science and Technology MISiS, 4 Leninskiy Prospekt, 119049 Moscow, Russian Federation

[4] Department of Physic, ITMO University, 49 Avenue Kronverksky 197101 St. Petersburg, Russian Federation

[5] Joint Institute for Nuclear Research, 6 St. Joliot-Curie 141980 Dubna, Russian Federation

[6] Dubna State University, 19 St. Universitetskaya 141982 Dubna, Russian Federation

[7] Ernst-Abbe-Hochschule Jena, 2 St. Carl-Zeiß-Promenade 07745 Jena, Germany

[8] Leibniz Institute of Photonic Technology, 9 St. Albert-Einstein-Straße 07745 Jena, Germany

[9] Department of Physic, North-Ossetian State University, 46 St. Vatutina, 362025 Vladikavkaz, Russian Federation

[10] Photonics Initiative, Advanced Science Research Center, 85 St. Nicholas Terrace, 10031 New York, United States

[11] Physics Program, Graduate Center City University of New York, 85 St. Nicholas Terrace 10031 New York, United States

[12] Department of Electrical Engineering, City College of New York, 85 St. Nicholas Terrace 10031 New York, United States

Correspondence to: D. Yakimchuk, dim2yakim@gmail.com

Abstract

Surface-enhanced Raman spectroscopy (SERS) is a promising optical method for analyzing molecular samples of various nature. Most SERS studies are of an applied nature indicating a serious potential for their application in analytical practice. Dendrite-like nanostructures have great potential for SERS, but the lack of a method for their predictable production significantly limits their implementation. In this paper, a method for controllable obtaining spatially

separated, self-organized and highly-branched silver dendrites via template synthesis in pores of SiO_2/Si is proposed. The dendritic branches have nanoscale roughness creating many plasmon-active "hot spots" required for SERS. The first held 3D modeling of the external electromagnetic wave interaction with such a dendrite, as well as experimental data, confirm this theory. Using the example of a reference biological analyte, which is usually used as a label for other biological molecules, the dendrites SERS-sensitivity up to 10^{-15} M was demonstrated with Enhancement factor of 10^8. The comparison of simulation results with SERS experiments allows distinguishing the presence of electromagnetic and chemical contributions, which have a different effect at various analyte concentrations.

I. Introduction

Raman spectroscopy – a measurement of the inelastic light scattering from a molecule with quantized vibrational signature – is a highly innovative technique of modern biomedical analysis, clinical and biological studies[1]. These areas have been experiencing a fast development, which has last for more than 40 years after the discovery that inherently weak Raman signals can be significantly enhanced for molecules adsorbed onto a rough metal surface. This effect, which can be attributed mainly to strong electric field enhancement around subwavelength metal roughness, is called Surface-Enhanced Raman Scattering (SERS)[2–5] and has been demonstrated for various plasmonic structures, including plasmonic nanoantennas[6], dimers with sub-10-nm gaps[7], disordered nanoparticle clusters, metamaterials, and metasurfaces[8].

Electromagnetic mechanisms usually provide the primary role in SERS amplification. Excitation of surface plasmons, i.e. coherent oscillations of free electrons at the metal-dielectric boundaries, causes regions of a strong electric field (hot spots) arising near metal nanostructures and at the junctions between them[9–11]. The SERS enhancement factor caused by this electric field localization is roughly proportional to the fourth power of the electric field amplitude. Subsequent analysis has shown that SERS is inherent not only to metals, such as copper (Cu)[12], silver (Ag)[13], and gold (Au)[14] but also to resonant all-dielectric nanostructures[15], demonstrating the universal nature of this effect, associated with the local electric field enhancement. However, in some cases the chemical contribution is a factor responsible for the sharp growth of the Raman

scattering cross-section due to the interaction of the analyte molecule with the metallic surface[16–19].

Tremendous progress in the area of Raman-based sensors led to the creation of the surfaces allowing Raman signal detection from a few or even single molecules[20]. The SERS enhancement factor (*EF*), which is usually defined as

$$EF = \frac{I_{SERS}}{C_{SERS}} \frac{C_R}{I_R},$$ (1)

has been demonstrated to be as large as 10^5-10^{11} (cf. Ref. [21]). Here, I_{SERS} stands for the Raman intensity obtained for the SERS substrate under a certain analyte concentration C_{SERS}, and I_R corresponds to the Raman intensity obtained under non-SERS conditions at analyte concentration C_R.

However, the adoption of SERS remains limited, to a great extent due to the fabrication difficulties of effective and affordable nanostructured plasmonic SERS surfaces. So far, SERS substrate fabrication techniques include lithography[7], laser ablation[22], templated electrodeposition[23], wet chemistry[24,25] and self-assembly[8,26]. The self-assembly technique is often considered the most promising because of its simplicity, cost- and time-effectiveness. For example, based on this approach, highly-branched dendritic nanostructures with sub-10-nm gaps between neighboring branches can be fabricated[27–29]. However, self-assembly techniques lack control over resulting structures. Thus, despite relatively satisfactory results[30], regularly reproducible detection of ultra-small concentrations of the analyte (in particular single molecules) using dendrites was not demonstrated. The main problem is related to the formation of bulk agglomerates[27,31–33], which limit stable detection at ultra-low concentrations of molecules due to the analyte penetration into the interior of such structures. As a result, the excitation laser does not access the analyte localization region and, consequently, the signal from the analyte is poorly recorded.

For that reason, such a problem can be solved by the spatial separation of nanostructures using porous templates: polymer track membranes, anodized aluminum oxide, porous silicon, etc.[34–37]. The formation of metallic nanostructures in the pores matrix is usually carried out using two methods: electrochemical deposition and electroless galvanic displacement. The first method is used to produce nanostructures filling the pore volume

(for example, in the formation of nanorods)[38], and the second – when it is required to realize individual nanoparticles or thin metallic layers on the pores surface[39].
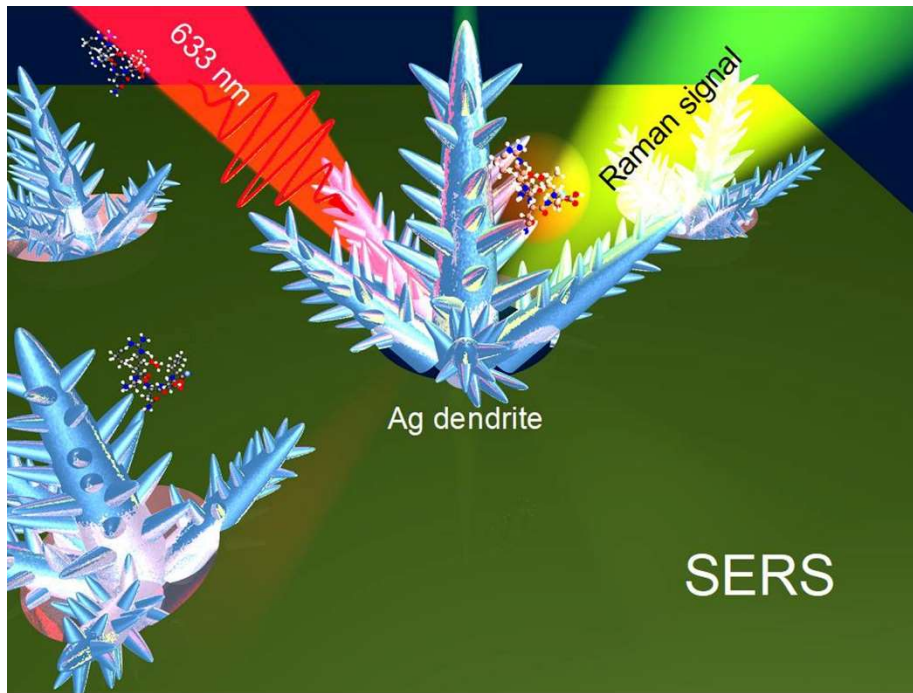
Fig. 1. Schematic representation of enhanced Raman scattering from a molecule nearby a silver dendrite.

In this paper, we develop and demonstrate a novel technique for the fabrication of spatially separate silver dendrites, presented schematically in *Figure 1*, via self-organization of Ag nanostructures in pores of SiO_2/Si templates. We investigate the microstructure, morphology, optical features and SERS properties of fabricated nanostructures. Also, we show that observed templates allow us to achieve a SERS enhancement factor of $\sim 10^8$ with a single molecule detection possibility ($\sim 10^{-15}$ M) of Ellman's reagent, which usually used as a label for others biological molecules.

II. Materials and methods

As templates for synthesis of silver dendrites, swift heavy ion-track porous SiO_2 matrix on *p*-type silicon substrate (12 Ohm·cm with orientation <100>) were used with a 170 nm thick silicon oxide layer and pore sizes of 800 nm. The procedure of obtaining porous SiO_2/Si templates are described in our previous paper[36]. The parameters of porous

template were determined using ellipsometry[40,41].The SiO_2/Si pore density over the surface was found to be 10^7 cm^{-2} according SEM studies determined by ImageJ[42].

The formation of Ag nanostructures in the pores of SiO_2 template on the Si substrate was carried out by electroless galvanic displacement method using an aqueous solution of Ag nitrate ($AgNO_3$) and hydrofluoric acid (HF), which dissociates in water into individual cations and anions (Ag^+, NO_3^-, H^+, F^-) as was published in our previous publication[43]. The resulted ions participate in three parallel processes[44,45]: electrochemical reduction of $[Ag]^+$ ions to a metallic silver state on Si or metal [Eq. (2)] with simultaneous anodic and cathodic oxidation of Si [Eq. (3)], and also SiO_2 dissolution in hydrofluoric acid [Eq. (4)]. Schematically, the processes taking place in the pore of the SiO_2/Si template are shown *in Figure 2*.

$$4Ag^+ + Si + 6F^- \rightarrow 4Ag + SiF_6^{2-}, \quad Si + 6HF \rightarrow H_2SiF_6 + 4H^+ + 4e^-,$$
$$Ag^+ + e^- \rightarrow Ag, \quad H_2 \rightarrow 2H^+ + 2e^-. \tag{2}$$

$$Si + 2H_2O \rightarrow SiO_2 + 4H^+ + 4e^-. \tag{3}$$

$$SiO_2 + 6HF \rightarrow H_2SiF_6 + 2H_2O. \tag{4}$$
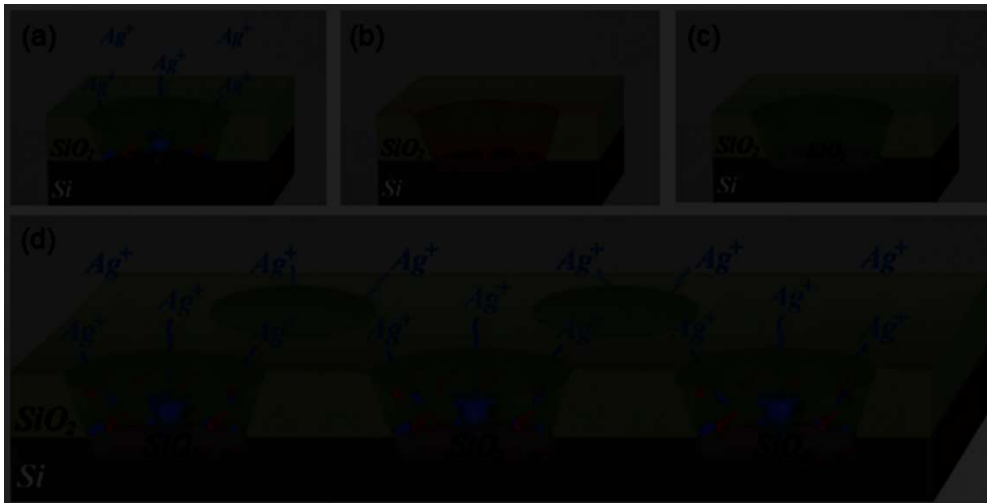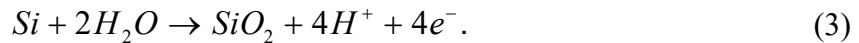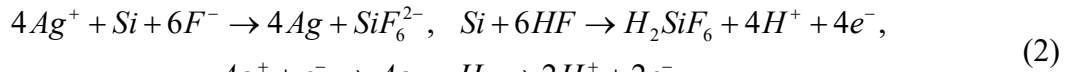
Fig. 2. Schematic representation of the processes involved in the reduction of $[Ag]^+$ ions occurring in pores of a template SiO_2 on Si: (a) Ag reduction; (b) SiO_2 etching; (c) Si oxidization; (d) all processes simultaneously.

Scanning electron microscopy (SEM, Carl Zeiss ULTRA 55, FE-SEM) was chosen to characterize the surface morphology of the obtained samples.

The EBSD (Electron Back-Scatter Diffraction) analysis of the samples was performed using a scanning electron microscope equipped with a Schottky emitter (Zeiss Ultra 55)

and a high resolution EBSD camera (Bruker e-Flash[HR]) using an acceleration voltage of 20 kV at a nominal sample current of 1.5 nA, sample tilt of 60° with respect to the primary electron beam, and a scanning step width of 12 nm. The resolution of the Kikuchi patterns was 160×120 pixels applying a 10×10 binning and using integration times of 40 ms. There were no problems with charging issues. The data were evaluated using a commercial software package (Bruker Quantax; Esprit 2.1) as well as the MATLAB toolbox MTEX[46].

To clarify the crystal structure of silver dendrites, the X-Ray diffraction (XRD) patterns were measured using X'Pert Pro X-ray diffractometer from PANalytical B.V. in the Bragg-Brentano arrangement.

The chemical state of the formed nanostructures was determined by X-ray photoelectron spectroscopy (XPS) in ultrahigh-vacuum (10^{-9} mbar) by K-Alpha ThermoScientific system with a monochromatic X-ray source Al-K-alpha 1.486 keV. To neutralize the surface charge, a compensation gun was used. The density of data collection of high-resolution spectra was 0.1 eV.

The scattering properties (LSPR - Localized Surface Plasmon Resonance) of the metal nanostructures were recorded with a dark-field micro-spectroscopy similarly as in Ref.[47]. Briefly, the micro-spectroscopy system consisting of an upright microscope (AxioImager Z1m, Carl Zeiss) was combined with a fiber-coupled spectrometer (Spectra Pro 2300i, Princeton Instruments) and was used in the dark-field top illumination settings. The microscope was equipped with a color camera (AxioCam Mrc5, Carl Zeiss) to record the overview images of the samples. The scattering signal was recorded from a circular area with the diameter of 15 μm (10x objective; NA = 0.2, 150 μm diameter aperture in front of the collecting fiber) from the middle of the overview image. The scattering signals were corrected with respect to the background and lamp spectrum.

The SERS measurements were performed using commercially available confocal micro-spectrometer "Confotec CARS" (SOL Instruments Ltd., Belarus) setup equipped with several laser systems including a 633 nm laser[48]. During the measurements a 600 lines per mm grating was used with a spectral resolution of ~ 2 cm^{-1}, the same objective (Leica 100x, 0.9 N.A.) was employed for focusing the laser beam on the sample and for collecting the backscattered light. The laser power 50 μW within the exposure time of 1s was exploited. For the SERS studies, the Ellman's reagent $C_{14}H_8N_2O_8S_2$ (5,50-dithiobis-(2-nitrobenzoic acid)) or DTNB was used as a model analyte in different concentrations: 10^{-4} M, 10^{-7} M, 10^{-10} M, 10^{-13} M, and 10^{-15} M. DTNB is a popular marker

for various biological molecules. For registration of ultra-low concentrations (10^{-13} M and 10^{-15} M) of the analyte, 10×10 μm mapping was used. For comparing with SERS spectra Raman spectrum measured from 10^{-2} M of DTNB on the SiO_2/Si template without silver.

CST Microwave Studio is a full-wave 3D electromagnetic field solver based on finite-integral time-domain (FITD) solution technique. A nonuniform mesh was used to improve accuracy near the Ag nanorods where the field concentration was significantly large[49]. The SiO_2 substrate thickness has been taken to be 170 nm. The lengths of big and small dendritic were ~1130 nm and 170 nm, respectively. The thickness of the big and small dendrites was 180 nm and 70 nm, respectively. The radius of the rounded outgrowths was 53 nm.

III. Result and Discussion

All the pores of the ion-track SiO_2/*p*-Si template are filled with dendritic silver nanostructures as shown in *Figure 3a*. The SEM image of a single pore filled with silver nanostructures is presented in *Figure 3b*. The image reveals that the nanostructures have the form of dendrites containing the main trunk, lateral branches and many rounded outgrowths on them. Due to the presence of nanoscale inhomogeneities between dendrites branches, the formation of "hot spots" can be expected with the enhanced electric field, which can be used for boosting the SERS effect.
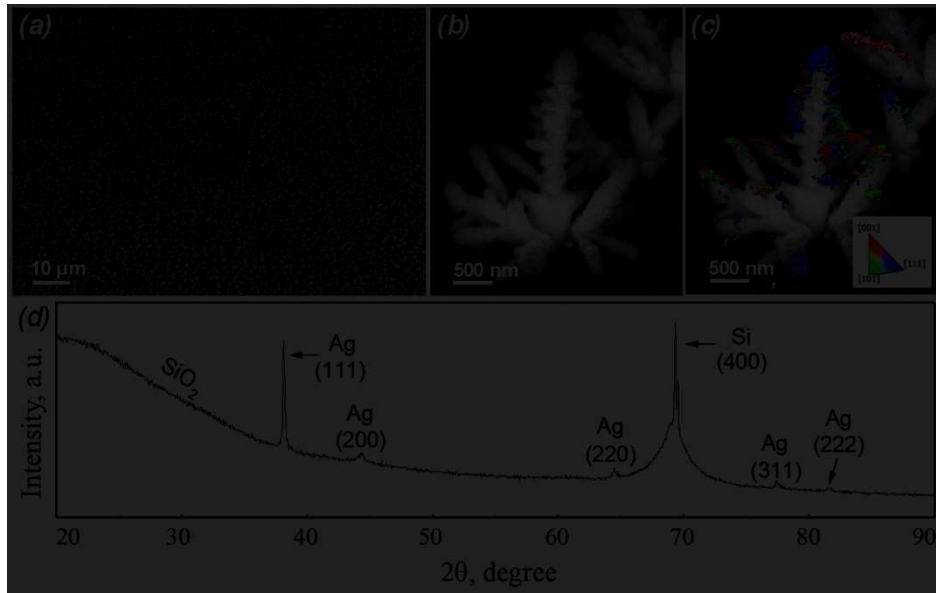
Fig. 3. Morphology and microstructure of observed $SiO_2(Ag)/Si$ structures: (a, b, c) overview and single feature SEM micrographs, (d, e) EBSD analysis of silver dendrite, (f) X-ray diffraction pattern; lattice parameter (*a*) of Ag dendrites is 4.0816 Å

The detailed structure of dendrites local features was evaluated by electron backscattered diffraction (EBSD). *Figure 3d,e* shows the EBSD orientation maps with inverse pole figure related color coding with regard to the sample surface normal direction z (IPFZ). For cubic systems, red color means that <100> crystal directions are parallel to the normal direction of the sample; green or blue colors are for <110> or <111> directions aligned to the normal direction, respectively. Our results suggest the presence of many blue spots around the main trunk which corresponds to the <111> crystal growth direction. Further investigations of grain boundary relations inside the nanostructure reveal that most of the grain boundaries are coincidence site lattice (CSL[50]) grain boundaries Σ3 (twin grain boundary) and few Σ9 (for more details see Methods).

The crystallinity of the silver dendrites in the pores of the SiO_2/p-Si template was determined using X-ray diffraction method. *Figure 3f* shows the XRD pattern of the produced structure. Unlike the typical diffraction patterns of silver dendrite[30,51], we observe a broad background signal coming from the amorphous SiO_2 layer. The peak at 2Theta about 69 deg corresponds to the signal from monocrystalline Si with highly broadened value due to the high defectiveness of the near-surface layers, which is the consequence of a template creating via ion-track technology on the irradiation stage with swift heavy ions. Ag dendrites have a cubic crystalline structure and are characterized by a set of reflexes from planes (111), (200), (220), (311) and (222). The broadened peak

of (200) reflex, also, points to the polycrystalline nature of the observed Ag precipitate. The high intensity of (111) reflex indicates the priority direction of crystallite growth along this direction that correlates with EBSD observations in *Figure 3 d,e.*

The result of XPS is presented in *Figure 4.* The asymmetric spectra for the Ag 3d line and the presence of low-intensity plasmon loss peaks confirm the metallic nature of the dendrites being formed[52].
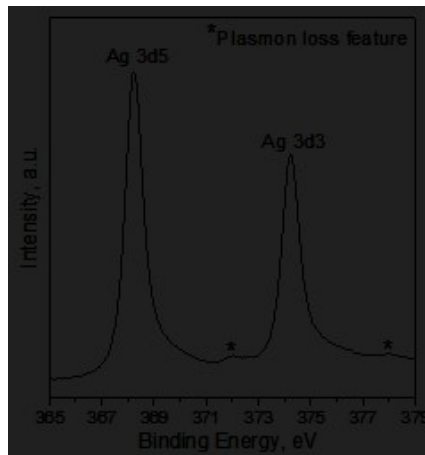
Fig. 4. XPS of spatially separated silver dendrites.

To investigate the optical properties of the fabricated dendritic Ag nanostructures numerically, we perform the full-wave simulations using commercial software CST Microwave Studio (*Figure 5a, b*). The simulation results indicate that the most intense "hot spots" are located between the neighboring dendrite branches, where the electric field enhancement reaches 12 as shown in *Figure 5b*. It is known that the SERS enhancement factor caused by electric field localization is roughly proportional to the fourth power of the electric field amplitude ($\sim E^4$). This gives us an estimation for the enhancement factor of $\sim 10^4$.
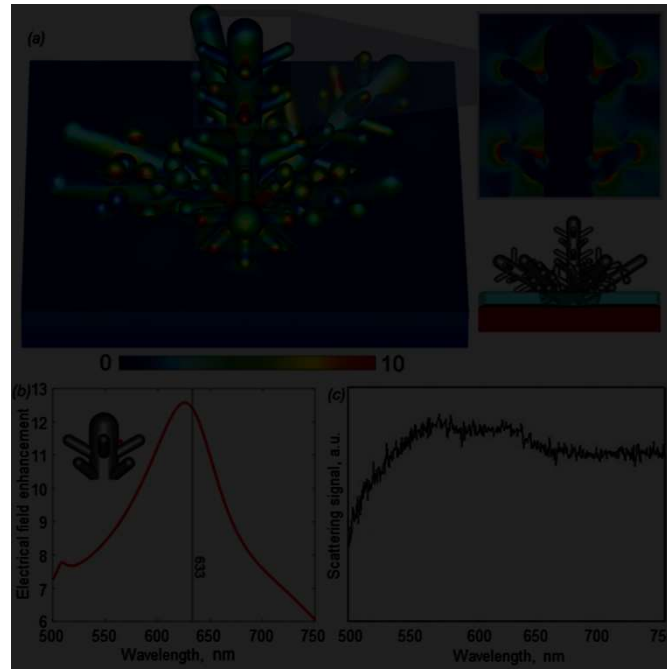
Fig. 5. (a) Distribution of the electric field over the surface of silver dendrite located in the pore of the SiO$_2$/Si template (E – local field, E_0 – incident field). (b) Electrical field enhancement spectrum in the point indicated by the inset. (c) Scattering spectrum of the dendritic nanostructures in the pores of the SiO$_2$/Si template.

The typical scattering spectrum (for more details see Methods) of the dendritic nanostructures is shown in *Figure 5c*. The complexness of the structure gives rise to spectral broadening of the measured scattering spectra[43]. Moreover, the scattered light-collecting area has a radius of 15 μm, and hence each spectrum is averaged over ~50 nanostructures, which causes its additional broadening. As a result, the scattering spectrum in *Figure 5c* does not exhibit sharp peaks in the range of 500 – 750 nm with a broadband resonant behavior nearby excitation wavelength (633 nm).
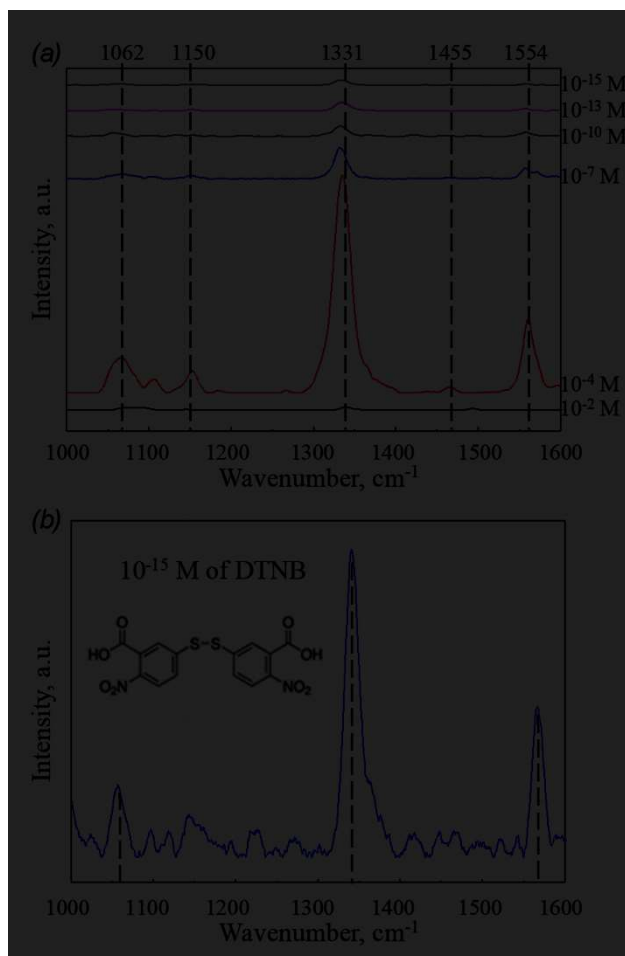
Fig. 6. (a) Raman spectrum for a dried alcohol solution of DTNB with the concentration of 10^{-2} M (black curve), as well as SERS spectra obtained at $\lambda = 633$ nm excitation from spatially separated Ag dendrites for analyte concentrations of 10^{-4} M, 10^{-7} M, 10^{-10} M, 10^{-13} M, and 10^{-15} M. (b) Zoomed SERS spectrum of DNTB with the concentration of 10^{-15} M.

Next, in order to demonstrate the performance of the resulting structures as a sensor, the SERS measurements using DTNB as a model analyte were performed (for details see Methods). *Figure 6* summarizes the obtained results. We attributed the observed most intense bands at 1062, 1150, 1331, 1555 cm^{-1} to the DTNB[53] analyte. The evolution of SERS spectra shows the possibility of detection of ultra-low concentrations of the model DTNB analyte by applying localized silver dendrite nanostructures, which correspond to EF at least 10^8.

According to modern concepts of Raman signal amplification mechanisms by plasmonic nanostructures, the highest amplification of the Raman signal occurs in "hot spots" due to the increased electromagnetic field strength in these places (figure 5a). The closer the molecule under study is to the "hot spots", the more intense the signal is recorded. However, given the fact that each dendrite has a large number of 'hot spots', signal

amplification by means of an electromagnetic mechanism is determined by all such places simultaneously. Even taking into account this fact, the obtained result of the amplification of the Raman signal is orders of magnitude higher than the numerical calculation. The EF value of 10^8 exceeds by several orders of magnitude the results of numerical simulations. We believe that this indicates the existence of a strong chemical contribution to SERS enhancement. This contribution can be caused by the following mechanisms: a change in the polarization of the molecule[16,17] (static charge transfer, causing an amplification up to 10 times) and the transition of a charge from a molecule to a metal (or vice versa) with the formation of a new metal-molecule bond, analyte creates new allowed energy levels[17,19,54]. The energy difference of these levels coincides or lies near the energy of exciting wave, which leads to resonant Raman scattering. It is known that such a mechanism can provide the amplification of $\sim 10^2$-10^3 [55] and even more[56]. Thus, the cumulative gain factor 10^8 is determined by the electromagnetic ($EF_{e.m.}$) and chemical (EF_{chem}) contributions[57,58]:

$$EF = EF_{e.m.} \times EF_{chem}. \qquad (5)$$

The appearance of new allowed levels in the energy spectrum of the molecule can lead to differences in comparison with the Raman spectrum of a bare analyte. Indeed, our results show (*Figure 6a*) that the main lines are shifted to the blue side and with decrease in the analyte concentration this effect gets enhanced. This behavior of the SERS spectra can be explained in the following way. With a sufficient amount of analyte molecules, both amplification mechanisms are involved: electromagnetic, which does not affect the spectrum change, and chemical, which causes the shift of the combination bands and is noticeably weaker than the electromagnetic one. With a decrease in the analyte concentration, the role of the electromagnetic mechanism is weakened, because fewer molecules get into "hot spots". Molecules, which still fall into these regions, fit closely to the metal and at several angstroms distances create a molecular-metal complex with silver. Thus, the molecule gets additional allowed energy levels. For that reason, the resonant transitions between these levels can also be enhanced by the electromagnetic mechanism. A decrease in concentration leads to the fact that molecules that fall into "hot spots" at distances of several tens of nanometers from metal do not form a bond with the silver surface. This is a consequence of the dominant effect of the chemical contribution to the SERS spectrum and a more noticeable shift in the combination lines.

Note that the formation of new molecule-metal complexes can occur not only in "hot spots", but also in other regions of the metal, which also affects the characteristic shape of the SERS spectrum with a decrease of the electromagnetic mechanism role.

There are various ways to create SERS substrates with plasmon-active metal inclusions in modern literature. For example, a highly sensitive SERS substrate was also demonstrated by Kumar et al.[59] and Sharma at al.[60]. They have enough sensitivities for detection ultra-low concentrations of target molecules and they also have a number of limitations associated with the complexity of manufacturing such substrates. The ion-track technology used in this work to create the SERS substrates is well suited for research purposes because it allows controlling template pore diameter very simple. The pore diameter is very important for obtaining spatially separated silver dendrites because this parameter influences the diffusion-limitation processes in the pores on the silver structures growing stage that is necessary for growth of dendrites. We will discuss this more detail in future work where we will consider silver morphology dependence on template pore diameter. In this work the presented results made it possible to determine that it is necessary to use templates with pore diameters of 800 nm for the growth of spatially separated silver dendrites. To obtain such pore diameters, classical lithography is also well suited. Therefore, in the future, this technique can be used to obtain ordered arrays of silver dendrites. Obtaining ordered silver nanostructures will not influence *EF* because "hot spots" arranged randomly on the dendrites. However, ordered structures are still relevant[61] because it will increase the analytical usefulness of SERS active substrates.

IV. Conclusions

Spatially separated Ag dendritic nanostructures in the pores of the ion-track template SiO_2/Si were synthesized using directed self-organization of Ag in a limited volume. Microstructure and optical features of $SiO_2(Ag)/Si$ nanostructures have been studied numerically and experimentally. It has been shown that the Ag nanostructures have the form of dendrites. The SERS measurement results indicate the possibility of ultra-low analyte concentration detection, comparable to the concentrations of single molecules. The high sensitivity of the fabricated structures is justified by the coexistence of electromagnetic and chemical contributions to the Raman signal amplification. The modeling of the electromagnetic wave interaction with dendrites indicates that the appearance of "hot spots" occurs in places of twinning (intergrowth of the branches of

the dendrite). The fabricated dendrites have a large number of "hot spots" with an electric field enhancement factor of 12. The random distribution of "hot spots" on a dendrite leads to its broadened scattering spectrum. We strongly believe that the simplicity, reproducibility, and scalability of the presented method for the formation of spatially separated dendrites make it promising for various vital applications in photonics, chemistry, and biology.

Acknowledgments

References

[1] C. Krafft, I.W. Schie, T. Meyer, M. Schmitt, and J. Popp, Chem. Soc. Rev. **45**, 1819 (2016).

[2] M. Moskovits, Journal of Raman Spectroscopy **36**, 485 (2005).

[3] K. Kneipp, H. Kneipp, I. Itzkan, R.R. Dasari, and M.S. Feld, Journal of Physics: Condensed Matter **14**, R597 (2002).

[4] C. Höppener and L. Novotny, Quarterly Reviews of Biophysics **45**, 209 (2012).

[5] D. Yakimchuk, E. Kaniukov., V. Bundyukova, S. Demyanov, V. Sivakov, Self-Organization of Plasmonic Nanostructures in Pores of Silica Template for SERS // Chapter 5 in "Fundamental and Applied Nano-Electromagnetics II" (Springer, Dordrecht), 2019, P. 75-90, DOI: 10.1007/978-94-024-1687-9_5.

[6] E. Ringe, B. Sharma, A.-I. Henry, L.D. Marks, and R.P. Van Duyne, Physical Chemistry Chemical Physics **15**, 4110 (2013).

[7] A. Gopalakrishnan, M. Chirumamilla, F. De Angelis, A. Toma, R.P. Zaccaria, and R. Krahne, ACS Nano **8**, 7986 (2014).

[8] S. Gwo, C.Y. Wang, H.Y. Chen, M.H. Lin, L. Sun, X. Li, W.L. Chen, Y.M. Chang, and H. Ahn, ACS Photonics **3**, 1371 (2016).

[9] G. Santoro, S. Yu, M. Schwartzkopf, P. Zhang, S. Koyiloth Vayalil, J.F.H. Risch, M.A. Rübhausen, M. Hernández, C. Domingo, and S. V Roth, Applied Physics Letters **104**, 243107 (2014).

[10] K. Kneipp, Physics Today **60**, 40 (2007).

[11] Y. Xia and D.J. Campbell, Journal of Chemical Education **84**, 91 (2007).

[12] E. Kaniukov, D. Yakimchuk, G. Arzumanyan, H. Terryn, K. Baert,A. Kozlovskiy, M. Zdorovets, E. Belonogov, and S. Demyanov, Philos. Mag. 97, 2268 (2017)

[13] T. V Shahbazyan and M.I. Stockman, *Plasmonics: Theory and Applications* (Springer Netherlands, Dordrecht, 2013).

[14] B. Sharma, R.R. Frontiera, A.-I. Henry, E. Ringe, and R.P. Van Duyne, Materials Today **15**, 16 (2012).

[15] A. Krasnok, M. Caldarola, N. Bonod, and A. Alú, Advanced Optical Materials **6**, 1701094 (2018).

[16] K. Kneipp, Journal of Physical Chemistry C **120**, 21076 (2016).

[17] L.L. Zhao, L. Jensen, and G.C. Schatz, J. Am. Chem. Soc. **128**, 2911 (2006).

[18] J.F. Arenas, M.S. Woolley, I.L. Tocón, J.C. Otero, and J.I. Marcos, The Journal of Chemical Physics **112**, 7669 (2000).

[19] L. Xia, M. Chen, X. Zhao, Z. Zhang, J. Xia, H. Xu, and M. Sun, Journal of Raman Spectroscopy **45**, 533 (2014).

[20] S. Nie, Science **275**, 1102 (1997).

[21] A. Balčytis, Y. Nishijima, S. Krishnamoorthy, A. Kuchmizhak, P.R. Stoddart, R. Petruškevičius, and S. Juodkazis, Advanced Optical Materials 1800292 (2018).

[22] S. V. Makarov, V.A. Milichko, I.S. Mukhin, I.I. Shishkin, D.A. Zuev, A.M. Mozharov, A.E. Krasnok, and P.A. Belov, Laser & Photonics Reviews **10**, 91 (2016).

[23] M.E. Abdelsalam, S. Mahajan, P.N. Bartlett, J.J. Baumberg, and A.E. Rusell, Journal of the American Chemical Society **129**, 7399 (2007).

[24] A.Y. Panarin, S.N. Terekhov, K.I. Kholostov, and V.P. Bondarenko, Applied Surface Science **256**, 6969 (2010).

[25] H. Bandarenka, K. Artsemyeva, S. Redko, A. Panarin, S. Terekhov, and V. Bondarenko, Physica Status Solidi (C) **10**, 624 (2013).

[26] D. Dong, L.W. Yap, D.M. Smilgies, K.J. Si, Q. Shi, and W. Cheng, Nanoscale **10**, 5065 (2018).

[27] P.R. Brejna and P.R. Griffiths, Applied Spectroscopy **64**, 493 (2010).

[28] T. Qiu, X.L. Wu, Y.F. Mei, P.K. Chu, and G.G. Siu, Applied Physics A: Materials Science and Processing **81**, 669 (2005).

[29] T. Qiu, X.L. Wu, J.C. Shen, Y. Xia, P.N. Shen, and P.K. Chu, Applied Surface Science **254**, 5399 (2008).

[30] M.M. Alam, W. Ji, H.N. Luitel, Y. Ozaki, T. Watari, and K. Nakashima, RSC Adv. **4**, 52686 (2014).

[31] W. Ye, C. Shen, J. Tian, C. Wang, C. Hui, and H. Gao, Solid State Sciences **11**, 1088 (2009).

[32] X. Sun, L. Lin, Z. Li, Z. Zhang, and J. Feng, Materials Letters **63**, 2306 (2009).

[33] C.K. Senthil Kumaran, S. Agilan, Dhayalan Velauthapillai, N. Muthukumarasamy, M. Thambidurai, A. Ranjitha, R. Balasundaraprabhu, and T.S. Senthil, Advanced Materials Research **678**, 27 (2013).

[34] S.J. Hurst, E.K. Payne, L. Qin, and C.A. Mirkin, Angewandte Chemie International Edition **45**, 2672 (2006).

[35] H. Masuda and K. Fukuda, Science **268**, 1466 (1995).

[36] E.Y. Kaniukov, J. Ustarroz, D. V Yakimchuk, M. Petrova, H. Terryn, V. Sivakov, and A. V Petrov, Nanotechnology **27**, 115305 (2016).

[37] H. Bandarenka, K. Girel, S. Zavatski, A. Panarin, and S. Terekhov, Materials **11**, 852 (2018).

[38] Y. Cao and T.E. Mallouk, Chemistry of Materials **20**, 5260 (2008).

[39] M. Wirtz and C.R. Martin, Advanced Materials **15**, 455 (2003).

[40] V. Bundyukova, E. Kaniukov, A. Shumskaya, A. Smirnov, M. Kravchenko, and D. Yakimchuk, EPJ Web of Conferences **201**, 01001 (2019).

[41] D. Yakimchuk, V. Bundyukova, A. Smirnov, and E. Kaniukov, Physica Status Solidi (B) **256**, 1800316 (2019).

[42] V. Bundyukova, D. Yakimchuk, E. Shumskaya, A. Smirnov, M. Yarmolich, and E. Kaniukov, Materials Today: Proceedings **7**, 828 (2019).

[43] D. Yakimchuk, E. Kaniukov, V. Bundyukova, L. Osminkina, S. Teichert, S. Demyanov, and V. Sivakov, MRS Communications **8**, 95 (2018).

[44] M. Abouda-Lachiheb, N. Nafie, and M. Bouaicha, Nanoscale Research Letters **7**, 455 (2012).

[45] W. Ye, Y. Chang, C. Ma, B. Jia, G. Cao, and C. Wang, Applied Surface Science **253**, 3419 (2007).

[46] R. Krakow, R.J. Bennett, D.N. Johnstone, Z. Vukmanovic, W. Solano-Alvarez, S.J. Lainé, J.F. Einsle, P.A. Midgley, C.M.F. Rae, and R. Hielscher, Proceedings of the Royal Society A: Mathematical, Physical and Engineering Science **473**, 20170274 (2017).

[47] N. Jahr, M. Anwar, O. Stranik, N. Hädrich, N. Vogler, A. Csaki, J. Popp, and W. Fritzsche, The Journal of Physical Chemistry C **117**, 7751 (2013).

[48] V.I. Fabelinsky, D.N. Kozlov, S.N. Orlov, Y.N. Polivanov, I.A. Shcherbakov, V. V. Smirnov, K.A. Vereschagin, G.M. Arzumanyan, K.Z. Mamatkulov, K.N. Afanasiev, A.N. Lagarkov, I.A. Ryzhikov, A.K. Sarychev, I.A. Budashov, N.L. Nechaeva, and I.N. Kurochkin, Journal of Raman Spectroscopy **49**, 1145 (2018).

[49] P.B. Johnson and R.W. Christy, Physical Review B **6**, 4370 (1972).

[50] A.P. Sutton; and R.W. Balluffi, *Interfaces in Crystalline Materials* (Oxford : Clarendon Press, New York, 1995).

[51] R. He, X. Qian, Y. Jie, and Z. Zhu, Chemical Physsics Letters **369**, 454 (2003).

[52] G.B. Hoflund, Z.F. Hazos, and G.N. Salaita, Physical Review B **62**, 11126 (2000).

[53] C.C. Lin and C.W. Chang, Biosensors and Bioelectronics **51**, 297 (2014).

[54] J.F. Arenas, M.S. Woolley, I.L. Tocon, J.C. Otero, and J.I. Marcos, Journal Of Chemical Physics **112**, 7669 (2000).

[55] S.K. Saikin, R. Olivares-Amaya, D. Rappoport, M. Stopa, and A. Aspuru-Guzik, Physical Chemistry Chemical Physics **11**, 9401 (2009).

[56] D.P. Fromm, A. Sundaramurthy, A. Kinkhabwala, P.J. Schuck, G.S. Kino, and W.E. Moerner, Journal of Chemical Physics **124**, (2006).

[57] S.K. Saikin, Y. Chu, D. Rappoport, K.B. Crozier, and A. Aspuru-Guzik, Journal of Physical Chemistry Letters **1**, 2740 (2010).

[58] A. Otto, Journal of Raman Spectroscopy **36**, 497 (2005).

[59] P. Kumar, R. Khosla, M. Soni, D. Deva, and S.K. Sharma, Sensors and Actuators B: Chemical **246**, 477 (2017).

[60] S. Sharma, V. Prakash, and S.K. Mehta, TrAC Trends in Analytical Chemistry **86**, 155 (2017).

[61] X. Zhang, Q. Zhou, J. Ni, Z. Li, and Z. Zhang, Physica E: Low-Dimensional Systems and Nanostructures **44**, 460 (2011).